Cellular thermometry considerations for probing biochemical pathways

Manjunath C. Rajagopal[1] and Sanjiv Sinha[1*].

[1]*Department of Mechanical Science and Engineering,*

University of Illinois at Urbana-Champaign, Urbana, IL 61801, USA.

ABSTRACT

Temperature is a fundamental thermodynamic property that can serve as a probe of biochemical reactions. Extracellular thermometry has previously been used to probe cancer metabolism and thermoregulation, with measured temperature changes of ~1-2 K in tissues, consistent with theoretical predictions. In contrast, previous intracellular thermometry studies remain disputed due to reports of >1 K intracellular temperature rises over 5 min or more that are inconsistent with theory. Thus, the origins of such anomalous temperature rises remain unclear. An improved quantitative understanding of intracellular thermometry is necessary to provide a clearer perspective for future measurements. Here, we develop a generalizable framework for modeling cellular heat diffusion over a range of subcellular-to-tissue length scales. Our model shows that local intracellular temperature changes reach measurable limits (> 0.1 K) only when exogenously stimulated. On the other hand, extracellular temperatures can be measurable (> 0.1 K) in tissues even from endogenous biochemical pathways. Using these insights, we provide a comprehensive approach to choosing an appropriate cellular thermometry technique by analyzing thermogenic reactions of different heat rates and time constants across length scales ranging from sub-cellular to tissues. Our work provides clarity on cellular heat diffusion modeling and on the required thermometry approach for probing thermogenic biochemical pathways.

INTRODUCTION

Biochemical reactions are often accompanied by enthalpy changes, resulting in local temperature changes. This renders temperature a physiological parameter of interest that can provide insights into biochemical pathways. For instance, extracellular thermometry has the potential to detect cancer [1] and thyroid-related diseases [2], and for understanding multiple metabolic pathways [3]–[6]. Such extracellular temperature changes originate in part from intracellular metabolic reactions. Hence, there has been a growing interest in intracellular thermometry [7]–[10] to probe sub-cellular metabolic pathways. However, studies using intracellular thermometry have been widely debated due to disagreements with theoretical predictions and potential measurement issues. For instance, previous studies [7], [11]–[17] report localized intracellular temperature rise > 1 K for 5 min or more, which exceeds theoretically predicted temperature changes [18]–[21] by several orders of magnitude. In some studies [7], [11]–[14], [16], such intracellular temperature rises were never reported to go back to room temperatures, arising questions on the theoretical plausibility [9], [18] of such results and their

*email: sanjiv@illinois.edu

This article is published in *Cell Biochemistry and Biophysics*. https://doi.org/10.1007/s12013-021-00979-w

measurement credibility. Potential measurement issues have been identified in certain fluorescence-based thermometry techniques and are widely discussed in other recent reports [18], [22]–[25]. On the other hand, the theoretical predictions of typical intracellular temperature changes remain disputed [18]–[21], [26]. Baffou et al [18], [19] estimated that the typical intracellular temperature changes don't exceed 10^{-5} K. Critics [9], [20], [21] have pointed out incorrect assumptions of heat source, cell thermal conductivity, and length scale of heat sources. Nonetheless, previous attempts [18]–[21], [26] to understand sub-cellular heat diffusion have been unable to explain the experimentally observed intracellular temperature changes [7], [11]–[16]. In contrast, at tissue length-scales, bioheat transport models [27], [28] with blood perfusion assumptions were previously used to predict the tissue-scale temperature changes, which are in good agreement with experimental results [4], [6], [27], [29]. Unlike tissue scale heat diffusion, sub-cellular heat diffusion modeling is less explored, and previous approaches to these two length-scales seem disconnected from each other. Therefore, there is a need for a unified approach to modeling heat diffusion in biological cells spanning length scales ranging from sub-cellular to tissues.

Here, we first reexamine the validity of the commonly used effective thermal conductivity (k_{eff}) approximation at cellular length-scales. Typically, in a cellular milieu, the spatial variations in thermal conductivity (k) are approximated as an effective thermal conductivity, k_{eff}, which is often reported as the thermal conductivity itself. Resistance to heat diffusion not only stems from the intrinsic material resistance, but also due to dissimilar material interfaces (Kapitza resistance, R''_{TIR}) which often results in a discontinuous temperature jump across the interface [30]. The cellular milieu is home to numerous dissimilar interfaces from biomolecular complexes such as proteins, cytoskeleton components, organelles, etc. that are suspended in the cytosol. Such biomolecular complexes with hydrophobic- or hydrophilic-water interfaces can result in R''_{TIR} of ~10^{-8} to 10^{-7} K.m^{2}W^{-1} [31]–[34] at a length-scale of ~50 nm. When interfaces dominate the overall thermal resistance, an effective thermal conductivity may no longer model heat diffusion behavior well. While the validity of k_{eff} has been questioned before [20], [26], this aspect has never been explored in detail. Here, we show that the effective thermal conductivity can become length-dependent if the interfacial resistances dominate, especially at cellular length-scales. We then incorporate the interfacial resistances in our model to calculate the expected temperature changes across sub-cellular to tissue length-scales. Our model helps to understand the typically expected temperature changes and consequently the thermometry requirements for thermogenic reactions of different timescales and heat rates. Overall, our work provides a cellular heat diffusion model and the cellular thermometry requirements, which are vital for applications such as nanoparticle heating of cryopreserved tissues [35], [36], thermal ablation of tumor cells [37]–[39], thermometry-based bioenergetics studies [9], [40]–[42], etc.

This paper is organized as follows. The Methods section discusses the cellular heat diffusion model, where we incorporate a cuboidal resistance network to capture the interfacial resistances of biomolecular complexes. We validate our resistance network and the heat diffusion model by comparing the results against the commonly used effective thermal conductivity approximation. Using the validated heat diffusion model, we first discuss the typical endogenous

temperature changes at sub-cellular and tissue length-scales. We then highlight the implications of the expected temperature changes in choosing a thermometry technique.

METHODS

Cellular heat diffusion model

Cells contain a variety of biomolecular complexes ranging from proteins and nucleic acids to membranes and cytoskeleton to organelles such as lysosomes and mitochondria. Due to collisions with other macromolecular compounds in the cytosol, molecular diffusion in the cytosol has been estimated to be four times smaller than pure water [43]. The diffusion of heat, on the other hand, has been relatively unexplored at sub-cellular length-scales [18]–[21], [26].

Heat transport in the cellular milieu can be assumed to be diffusive in nature, since the molecular mean free path in liquids is much smaller than 1 nm. However, the subcellular region contains biomolecular complexes that result in numerous dissimilar interfaces, where the diffusion approximation is no longer valid [44]–[46]. One of the commonly used techniques to model the thermal interfacial resistance at dissimilar surfaces is molecular dynamic (MD) simulations [47]–[52]. For instance, studies using non-equilibrium MD simulations have captured the effects of interface topography [53], curvature [52], size, bonding energy [49], etc. on the thermal interfacial resistance. On the other hand, continuum models such as finite element methods (FEM) approximate the temperature discontinuity across dissimilar interfaces using the interfacial resistance as an input parameter [48], [54]. Typically, the thermal interfacial resistances are either measured experimentally [33], [54] or calculated from MD simulations [48], [53]. MD based simulations are usually limited to confined domains of few nm^2- μm^2 and are also limited by the computational capacity to be able to model an entire cell. To this end, in this work, we model the heat transport in cells and tissues using finite element methods through COMSOL Multiphysics software. While FEM cannot intrinsically estimate the thermal interfacial resistances, we instead investigate heat transport for a range of possible interfacial resistances for the biomolecular complexes. We discuss the range of values for the interfacial resistance shortly.

We model heat flow using the transient heat diffusion equation,

$$\nabla.(k\nabla T) + \dot{Q}''' = \rho C_P \frac{\partial T}{\partial t} \tag{1}$$

where, T is the temperature, $\dot{Q}'''$ is the volumetric heat generation rate, ρ is the density, C_p is the specific heat, k is the thermal conductivity. Equation (1) is valid for diffusive heat transport across a range of sub-cellular to tissue length-scales. However, at sub-cellular length-scales, the material properties $k, \rho,$ and C_p are a strong function of the spatial location due to the suspended biomolecular complexes. Under steady-state conditions, the spatial variations of ρ and C_p can be ignored. In a typical experimental measurement, the spatial variations in k and the effects of

additional interfacial resistances are approximated by an effective thermal conductivity, k_{eff}, which is often reported as the thermal conductivity itself. Previous work [18]–[21], [26] typically used experimentally measured k_{eff} in a simplified version of Equation (1) to model the cellular heat diffusion and for predicting the expected temperature changes. Instead, in this work, we explicitly model the thermal interfacial resistance (R''_{TIR}) of biomolecular complexes by introducing a temperature discontinuity at their surface, given by,

$$\Delta T = \frac{R''_{TIR}\dot{Q}}{A} \tag{2}$$

where, $\dot{Q}$ is the rate of heat flow, and A is the surface area of the biomolecular complex.

Typical biomolecular complexes such as proteins are suspended in the cytosol with the hydrophilic side chains exposed to saline, while the hydrophobic chains are curled inside. Such hydrophilic-water interfaces are expected to have thermal interfacial resistance (R''_{TIR}) of ~10^{-8} $K.m^2W^{-1}$ [31], [32]. For a hydrophobic-water interface, the interface resistance is typically higher and is ~2×10^{-8} $K.m^2W^{-1}$ [33]. Highly hydrophobic materials such as carbon nanotubes have a thermal interfacial resistance of ~2×10^{-7} $K.m^2W^{-1}$ with water [34]. Such interfacial resistances can produce a considerable temperature change. For instance, if 1 nW of heat flows across a protein chain of 50 nm width with R''_{TIR}~10^{-7} $K.m^2W^{-1}$, the temperature change can be as high as ~20 mK across a length of 100 nm. Further, when the interfacial resistances dominate the overall resistance to heat diffusion, the effective thermal conductivity (k_{eff}) would be less than that of proteins (k_p~0.1-0.2 $Wm^{-1}K^{-1}$). This can happen at sub-cellular length-scales and has recently been observed in an intracellular effective thermal conductivity measurement [55], which reported a k_{eff}~ 0.07-0.13 $Wm^{-1}K^{-1}$. To accurately capture the heat diffusion at sub-cellular length-scales, Equation (2) must be used as a boundary condition at the surfaces of biomolecular complexes while solving Equation (1). Moreover, the topology of the biomolecular complexes must be established to be able to model the interfacial resistances. Therefore, in the following section, we introduce a generalized cubical topology for the biomolecular complexes.

A generalized resistance network

Figure 1a shows a partial picture of the cellular components across a ~0.1 μm^2 area near the cell wall [56]. The cytoskeleton components such as actin, intermediate filaments, and microtubules are roughly 6 nm, 10 nm, 25 nm in diameter [57]. A steady-state heat diffusion across this subcellular space is subjected to a thermal resistance from the medium (t/k_{med}), the intrinsic resistance of proteins in the filaments (t/k_p) and the interfacial resistances of the filaments (R''_{TIR}), where t is the corresponding thickness. The thermal resistance network in the cellular environment can be visualized as numerous pockets of polyhedrons (filled with water) surrounded by protein chains. This can be approximated as cuboidal pockets of medium surrounded by surfaces of protein with a lumped resistance R''_S, as shown schematically in Figure 1b. The validity and impact of this approximation are discussed later, but we first explain the physical meaning of this lumped

resistance R_S''. The resistance R_S'' can be assumed to be a lumped representation of all the intracellular components and their interfacial resistances. A mathematical representation of R_S'' is:

$$R_S'' \approx A \sum_i \frac{t_i}{k_{p_i} A_i} + \frac{R''_{TIR_i}}{A_i} - \frac{t_i}{k_{med} A_i} \tag{3}$$

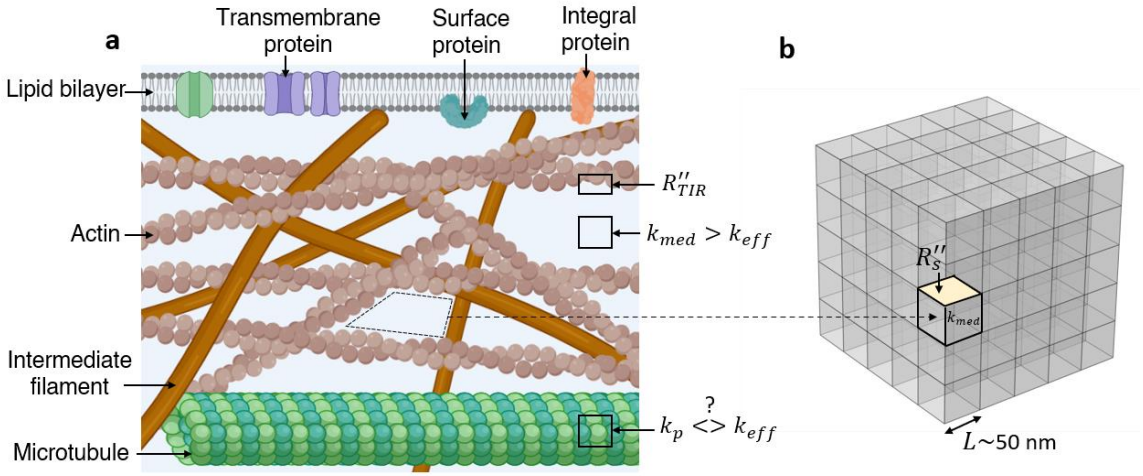

Figure 1 a) Schematic of typical cytoskeleton components in a roughly 0.1 μm^2 area near the cell wall. k_{eff} is the effective thermal conductivity of all the components shown here. If $k_p > k_{eff}$, the thermal interfacial resistance (R''_{TIR}) dominate the k_{eff}. b) A simplified representation of the thermal resistance network. The medium is assumed to have a thermal conductivity of k_{med}, surrounded by surfaces on all sides with a resistance of R_S'' (K.m^{2}W^{-1}).

where, t_i is the thickness of a lipid/protein/organelle i with a thermal conductivity k_{p_i}, effective surface area A_i, with an interfacial resistance R''_{TIR_i}, and A is the surface area of the individual unit (~L^2) along which R_S'' is borne (Figure 1b). The last term in Eqn. (3) accounts for the reduction in the medium's resistance due to displacement of the medium by the material i. Any advection thermal resistance can also be a part of Eqn. (3). We henceforth call this resistance R_s'' as the equivalent thermal resistance at a length-scale L, since from Eqn. (3) we can see that R_S'' is a strong function of the length-scale ~At_i/A_i. At a length-scale of L~50 nm, R_S'' is representative of the resistances from protein chains, whereas, at a length-scale L~50 μm, R_S'' represents all the proteins in the cell as an equivalent lumped resistance at the cell-wall. Thus, R_S'' can be higher at 50 μm than at 50 nm. We now discuss the implications of a cuboidal resistance network approximation. Unless stated otherwise, we assume in this work that the pockets are filled with a medium, whose k_{med} = 0.58 Wm^{-1}K^{-1}, corresponding to the thermal conductivity of water. The real picture could be better represented by a k_{med} that is < 0.58 Wm^{-1}K^{-1}, due to the dispersed proteins and ions, and R_S'' could be $\sum_i R_{TIR_i}$, instead of Eqn. (3). However, since an accurate spatial distribution of k_{med} and R''_{TIR} is not available for a heterogeneous cellular environment, we assume that all the additional resistances are lumped along the surface as R_S'' (Eqn. (3)). Further, we assume a rectilinear topology (cuboid) for the unit cell of the resistance network as shown in Figure 1b.

The real topology could be complex (with entangled resistance network and high interfacial resistances) or simpler (with a homogenous dispersion of proteins and low interfacial resistance). Our cuboidal resistance network may not be a unique representation, but we show in this work that it serves well as a general example to understand the cellular heat diffusion picture.

RESULTS

Revisiting the effective thermal conductivity approximation

We revisit the effective thermal conductivity approximation and use it to validate our cuboidal resistance network model. An effective thermal conductivity, k_{eff}, approximates the local thermal resistances such that under a known amount of steady heat (Q), the temperature change (ΔT) can be predicted using a single thermal property, k_{eff}. The effective thermal conductivity is a function of the type of heat input (line, surface, or volumetric) [58], and the location of the temperature measurement. Typically, the measured temperatures can be volume averaged (T_{v-av}), surface average (T_{s-av}), volume maximum (T_{v-m}), or surface maximum (T_{s-m}). For bio-heat transport studies, especially for thermometry-based bioenergetics studies, a useful and an often-measured parameter is the average temperature in a volume (T_{v-av}). The T_{v-av} is representative of an average temperature measured using fluorescent dyes, or dispersed nanoparticles. If the heat input is known (say, endogenous heat source, or laser), the average temperature change can be used to estimate the local effective thermal conductivity, k_{eff}[55], [59]. Thus, in this study, we assume k_{eff} as the effective (or measured) thermal conductivity calculated using the volume averaged temperature (T_{v-av}) for a known volumetric heat source. We later discuss how the location of temperature measurement and the type of heat source affect the effective thermal conductivity k_{eff}.

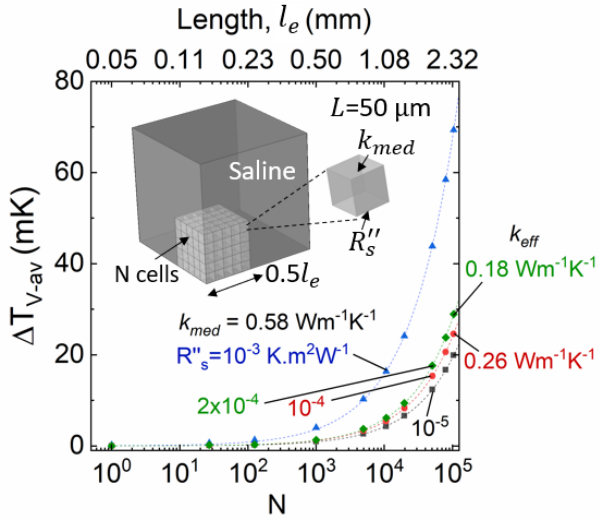

Figure 2. Volume averaged temperature change (ΔT_{v-av}) of the stack of cells is plotted against the number of cells, N, in the stack. The total edge length of the stack of cells is given by l_e, which is ~$(NL)^{0.33}$, where L is the length of each cell surrounded by R_s''. The ΔT_{v-av} are shown for 4

combinations of k_{med} and R_s'', as shown inside the graph. For lengths, l_e> 1 mm, the plotted ΔT_{v-av} also correspond to a stack of cells with an effective thermal conductivity, k_{eff}, as noted outside the graph using the corresponding colors. Each cell is assumed to release heat of 2.5 nW. Only 1/8th of the domain is shown in the schematic for clarity.

Using the above-mentioned definition of effective thermal conductivity, k_{eff}, we now discuss how the cuboidal resistance network's k_{eff} prediction compare against those that were previously measured experimentally. Consider a stack of N cuboidal cells (Figure 2), representing a multi-cellular tissue. Each cell has an edge length, L=50 μm, roughly corresponding to an adipose cell size [60]. The cells are assumed to be filled with a medium of thermal conductivity k_{med}, surrounded by an equivalent surface resistance, R_s''. The stack of cells is surrounded by saline. A constant outer surface temperature (20°C) is assumed at the saline far from the tissue. At large length scales, $l_e \gg R_s'' k_{med}$, where $N \to \infty$, the effective (or measured) thermal conductivity of the tissue can be analytically approximated as,

$$k_{eff} = \frac{L}{R_S'' + \frac{L}{k_{med}}} \tag{4}$$

We computationally confirm the effective thermal conductivity approximation (Eqn. (4)) using Figure 2. We use finite element simulations that were validated for interfacial resistance modeling in our previous work [40], [54], [61] and for modeling transients in the supplementary material. A nominal volumetric heat of 2.5 nW is assumed to be released per cell, which corresponds to a typical cell metabolism rate [41], [62]. We plot in Figure 2 the volume-averaged temperature change (ΔT_{v-av}) in the cell stack against the number of cells, N, in the stack. ΔT_{v-av} is plotted for different equivalent resistances, R_s'' from 10^{-3} to 10^{-5} K.m^{2}W^{-1}. We also plot the corresponding temperature changes without an equivalent resistance R_s'', but with an effective thermal conductivity k_{eff} (0.18 and 0.26 Wm^{-1}K^{-1}), for l_e> 1 mm, as marked outside the graph in Figure 2. We specifically choose a k_{eff} of 0.18 Wm^{-1}K^{-1} and 0.26 Wm^{-1}K^{-1} since previous studies report the effective thermal conductivity for adipose tissues to be in the range 0.18-0.26 Wm^{-1}K^{-1} [28], [63]. From Figure 2, we find that the calculated temperatures (ΔT_{v-av}) using k_{eff} of 0.18 Wm^{-1}K^{-1} and 0.26 Wm^{-1}K^{-1} are indistinguishable from the calculated ΔT_{v-av} for a cuboidal resistance network with k_{med}=0.58 Wm^{-1}K^{-1}, R_S'' of 2×10^{-4} and 10^{-4} K.m^{2}W^{-1}, respectively. In other words, a k_{eff}= 0.18-0.26 Wm^{-1}K^{-1} that was previously measured for adipose tissues is equivalent to a tissue made up of cells of L=50 μm each with a k_{med}=0.58 Wm^{-1}K^{-1} and $R_s'' =$ 2×10^{-4} – 10^{-4} K.m^{2}W^{-1}, respectively, as also estimated by Eqn. (4). Thus, the cuboidal resistance network consisting of k_{med} and R_s'' can capture the effective thermal conductivity approximation at tissue length-scales.

At sub-cellular length-scales, a recent report [55] measured the thermal conductivity to be 0.07-0.13 Wm^{-1}K^{-1} with a spatial resolution of 200 nm inside a cell. Since the measured k_{eff} is less than protein's thermal conductivity, k_p (~0.1-0.2 Wm^{-1}K^{-1}), the interfacial resistances (R_{TIR}'') possibly dominated at sub-cellular length-scales. We approximated the cellular heat diffusion picture to a cuboidal resistance network to explicitly account for the interfacial resistances (R_{TIR}'').

Consequently, a low k_{eff} can be explained using the cubic resistance network if the lumped resistance R_s'' is in the range 10^{-7}-10^{-6} K.m^{2}W^{-1} (Figure S2 in supplementary material) at L~ 50 nm. Therefore, the cuboidal resistance network can provide a reasonable approximation to the thermal conductivity across a range of sub-cellular to tissue length-scales.

Limitations of effective thermal conductivity approximation

The effective thermal conductivity, k_{eff}, is a function of the length-scale at which it was estimated (Figure 3), especially if the local thermal interfacial resistances dominate the total thermal resistance. If the local thermal resistances (R_s'') are in the order of 10^{-4} K.m^{2}W^{-1} at a length-scale of 50 μm, the effective thermal conductivity is a strong function of the length scale varying from 0.05 Wm^{-1}K^{-1} to 0.25 Wm^{-1}K^{-1}, over 50 μm to 2 mm length-scale. Figure 3 shows that the effective thermal conductivity can be as low as ~0.05 Wm^{-1}K^{-1} at cellular length-scales (<50 μm), which is in close agreement with a recent report [55] of intracellular k: 0.07-0.13 Wm^{-1}K^{-1}. We mark this experimentally reported thermal conductivity in red circle in Figure 3 at N~1. Similarly, for adipose tissues, the thermal conductivity is typically in the range 0.18-0.26 Wm^{-1}K^{-1} [28], [63], which is also highlighted in red in Figure 3 at larger length-scales (l_e~2 mm). Notably, our resistance network model can capture the thermal conductivity variation from sub-cellular to tissue length-scales. The data shown in black line in Figure 3 corresponds to our specific assumption of a cuboidal topology for the resistance network. In general, the true functional relationship between effective thermal conductivity and length-scale could be determined by mapping the true topology of the resistance network in the system. Our cuboidal topology serves as a generalized example to show that the local interfacial resistances can be responsible for the reduction in effective thermal conductivity at smaller length-scales.

The equivalent resistance (R_s'') is responsible for reducing the effective thermal conductivity at lower length-scales (Figure S2). The value of this resistance R_s'' scales directly with the length-scale (L), as evident from Eqn. (4). A resistance, R_s'', of ~10^{-4} K.m^{2}W^{-1} at a length-scale L=50 μm may seem high; however, it scales down to an equivalent resistance, R_s'' of ~10^{-7} K.m^{2}W^{-1} at a length-scale L=50 nm, where the contribution of R_{TIR_i}'' can no longer be ignored in R_S''. A resistance of 10^{-7} K.m^{2}W^{-1} is comparable to that of hydrophobic-water interfaces [33], [34]. At sub-cellular length scales ~50 nm, if the local resistance R_s'' is on the order of 10^{-7} K.m^{2}W^{-1}, k_{eff} can vary from 0.05 Wm^{-1}K^{-1} to 0.25 Wm^{-1}K^{-1} over length scales of 50 nm to 2 μm (Figure 3). The interfacial resistance (R_{TIR}'') contribution to the lumped resistance R_S'' cannot be ignored at a length-scale l_e where $R_S'' \sim \sum_i R_{TIR_i} \sim l_e/k_p$ could be all in similar orders of magnitude. The exact length-scale l_e at which R_{TIR}'' dominates cannot be known for certain since we do not have any information on the TIR of multiple interacting protein chains or organelles.

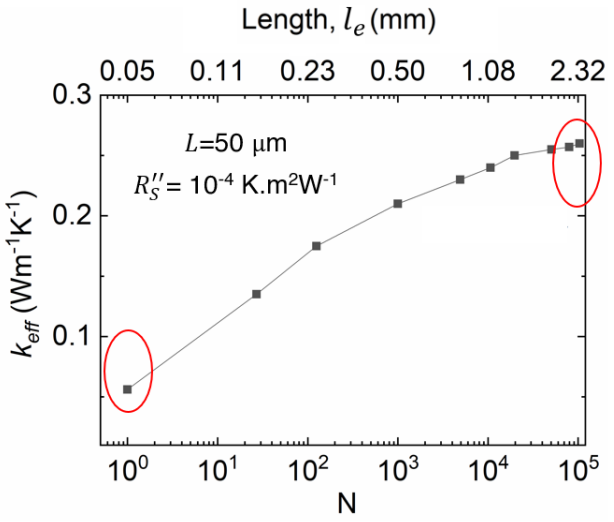

Figure 3. Effective thermal conductivity (k_{eff}) is a function of the length-scale at which it is measured. We find the k_{eff} at each length scale, l_e, by matching the volume averaged temperature (T_{v-av}) for a stack of N cells with a resistance network of k_{med} and R_s'' to that of a stack with a k_{eff}. We assumed a constant volumetric heat of dissipation per cell. The region in red corresponds to some of the previous experimental data points [28], [55], [63].

The effective thermal conductivity, k_{eff}, is also dependent on the type of input heat source (volumetric or surface), and the location of the measured temperature. For bioenergetics studies, we assumed that a k_{eff} is typically measured using the average temperature change over a volume (ΔT_{v-av}) for a known volumetric heat input, Q. However, if the length-scale l_e of effective thermal conductivity k_{eff} measurement is in the order of L, which is the length-scale of local resistances (R_s''), the k_{eff} approximation may fail to capture the true temperature distribution, as shown in Figure 4. If k_{eff} is used, we denote the temperature changes as ΔT_{keff}, calculated using the known k_{eff}. Similarly, we denote the temperature changes calculated using the cuboidal resistance network (k_{med} and R_s'', Figure 1b) as ΔT_R. We find from Figure 4 that if the effective thermal conductivity is defined using the average temperature (ΔT_{v-av}), the local surface temperatures (ΔT_{s-m}) can be higher by 67%, or the overall maximum temperature (ΔT_{v-m}) can be lower by 51% in comparison to the true temperature changes (ΔT_R). Only at length-scales $l_e \gg L$, as shown in Figure 4, an effective thermal conductivity can capture the true temperature distribution.

We note here that we assumed the true temperature change to be ΔT_R (in Figure 4), corresponding to a cuboidal resistance network, which is one of the many possible topologies. The real picture could be worse (with entangled resistance network and high interfacial resistances) or better (with a homogenous dispersion of proteins, low cell packing density, and low interfacial resistance). The former is more likely since it supports the reduction in the effective thermal conductivity to values below that of typical proteins (Figure 3).

Typical calorimetry techniques [41], [42] for biological cells measure the temperature of the surrounding medium to estimate the total heat released from a cell. Such techniques inherently assume an effective thermal conductivity for the cell and the surrounding medium during the calibration of the thermal resistance of the calorimetry cell using an external heater. We discussed in this section that the effective thermal conductivity is a function of the location of the heat source, the location of the measured temperature, and the local interface resistance network (Figure 4). Since the resistance to heat flow for an external heater may be different in comparison to any intracellular heat sources, previously reported calorimetry techniques [41], [42] may not be able to capture the true intracellular heat release via externally measured temperatures.

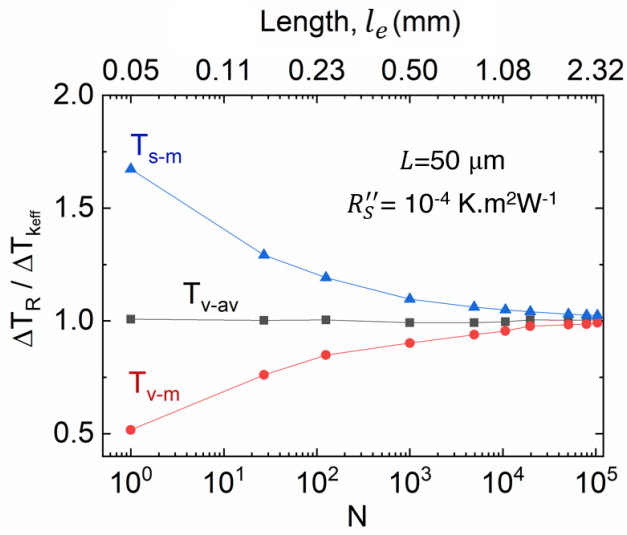

Figure 4. Effective thermal conductivity (k_{eff}) may not capture the temperature distribution at smaller length-scales. We use the k_{eff} shown in Figure 3, for this plot. s-m: surface maximum, v-m: volume maximum, v-av: volume average.

Typical temperature changes

In the previous sections, we developed a cuboidal resistance network that offers a generalizable way to model the interfacial resistances. The topology of the resistance network and the absolute value of the resistances may vary widely across cell lines. In this section, we explore the typical endogenous temperature changes for a range of length-scales and interfacial resistances. An estimate of the typical temperature changes can help determine the required sensitivity of measurement techniques to measure such temperature changes.

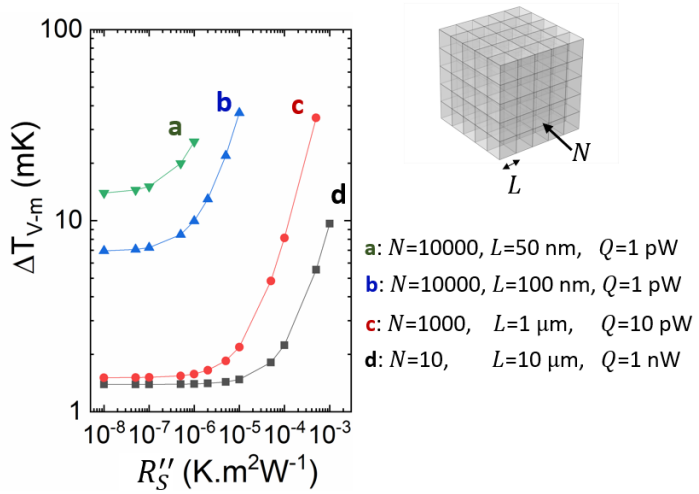

Figure 5. Maximum localized temperature changes in sub-cellular compartments due to a total endogenous heat release rate of 10 nW. We plot this for a range of possible equivalent resistances, R_S'', at a length-scale L. The notations a, b, c, d correspond to different types of subcellular compartments. A conservative thermal conductivity of 0.1 Wm^{-1}K^{-1} was assumed for the subcellular compartments and the surrounding medium (cytosol).

Sub-cellular localized temperature changes

In this section, we estimate the localized temperature changes in sub-cellular compartments due to endogenous heating. Endogenous heat release in individual cells is typically in the range of 1–10 nW in a 50 µm diameter cell (~1-20 kW/m^3) [28], [41], [62]. We consider a few different scenarios (listed in Figure 5) each representing different sub-cellular compartment sizes, but all producing the same 10 nW of total heat. For instance, scenario *a* has 10,000 compartments each producing a heat Q=1 pW and has a length-scale L= 50 nm roughly corresponding to individual protein chains. On the other hand, the scenario *c* has 1,000 compartments each producing a heat Q=10 pW and has a length-scale L= 1 µm, roughly corresponding to that of mitochondria. In Figure 5, we show the maximum localized temperature changes in such sub-cellular compartments. We only plot the temperature changes for a range of possible equivalent resistances R_S''. For instance, we do not plot the temperature changes in scenario *a* for R_S''> 10^{-6} K.m^{2}W^{-1}, since it is unlikely for protein chains of 50 nm length-scale to have such resistances. The volumetric heat rate for the scenarios shown in Figure 5 are in the range ~1- 8000 MW/m^3. Despite such a high volumetric heat release rate, the localized temperature changes in a cell are expected to be < 0.1 K. This is contrary to certain previous studies that report intracellular organelles to be ~1 K higher than the cytosol [7], [17]. The intracellular temperature changes can be greater than 0.1 K if exogenous stimulants [9], [36], [64], [65] such as proton uncouplers (BAM15, CCCP, FCCP), laser, resonating magnetic nanoparticles, etc. are used to increase the heat released in cells by several orders of magnitude above endogenous conditions. Moreover, transient endogenous temperature fluctuations in a 10 nm sub-cellular compartment can be up to ~1 K, but it can only occur over a timescale of 0.1 ns, which could be averaged-out by most measurement techniques [26]. Overall,

to measure endogenous and localized temperature changes in intracellular regions, the measurement technique is required to have a detection limit $\ll$ 100 mK.

Tissue-scale temperature changes

A few nanowatts of intracellular heat cannot raise the local temperature in an isolated cell by a few K as evident from Figure 2 and Figure 5. However, it is well known that brown adipose tissue (BAT) cells contribute toward increasing the local tissue temperatures by 1-2 K [4], [5], especially under cold-induced conditions. In this section, we systematically show how the temperature changes increase from a few mK in a single isolated cell to 1-2 K in tissues through our cuboidal resistance network for cells. We also compare our results against a bioheat transport model that was previously developed for tissues.

For a nominal heat of 2.5 nW per cell, we previously discussed in Figure 2 that the average temperature change increases with the number of cells, N. The temperature changes, ΔT_{V-av}, in Figure 2 roughly follows a power-law, $\Delta T_{V-av} \propto N^{\gamma}$, where $\gamma = 0.63$-0.67, which is consistent with previous analytical estimates [18], [66]. By extrapolating this fit, in Figure 6a, we calculate the corresponding temperature changes at tissue length-scales of ~20 mm. The thermal conductivity of adipose tissue is typically in the range of 0.18-0.26 $Wm^{-1}K^{-1}$. The corresponding ΔT_{V-av} is expected to be in the range of 2-4 K for a tissue of size ~ 20 mm (Figure 6a). We compare this prediction to a 3D bio-heat transport model that was developed for tissues to include the effects of blood perfusion. Details of this model are available in previous studies [27], [28], and also in the supplementary material. Briefly, the bioheat transport model accounts for volumetric metabolic heat production (Q'''_{met}) at tissues and blood associated thermoregulation (Q'''_{blood}). The blood perfusion rate is expressed as ω_b in s^{-1}. The volumetric heat supplied or removed by the blood is then given by, $Q'''_{blood} = \rho_b \omega_b C_b (T_b - T)$, where C_b is the specific heat capacity, ρ_b is the density of the blood, T_b is the arterial blood temperature, and T is the local tissue temperature. In Figure 6b, we use the bio-heat transport model to calculate the expected temperature changes in brown adipose tissue (BAT) deposits during a cold-induced ($T_{ambient}$=15°C) thermogenesis. BAT volumes vary depending on age, location, and weight of the individual. Here, we choose a 2 cm^3 ellipsoidal BAT as representative of supraclavicular region [28], [67], [68]. We used previously reported thermal and physical properties for blood, fat (BAT and WAT), and muscle, which we also summarize in Table S1 in the supplementary material. Our previous estimation of ΔT_{v-av}~2-4 K rise in a stack of cells (Figure 6a) is equivalent to a scenario in BAT (Figure 6b, Q=2-3 nW/cell) with no blood perfusion. Notably, we were able to predict the temperature change in tissues by using a framework built from single cells (with k_{med} and R''_s along a cuboidal resistance network) each producing ~2.5 nW of heat. The ΔT from a stack of cells (Figure 6a) did not include the effects of blood transport. Blood perfusion is responsible for the nutrient transport required to sustain the thermogenesis. Considering the effects of blood perfusion, we expect the tissue's temperature to rise by ~1 K (Figure 6b). This is also consistent with previous experimental reports that studied thermoregulatory neuronal circuits and report a maximum temperature change in the order of ~1-2 K in BAT deposits [4], [5]. Even though intracellular temperature changes are $\ll$ 0.1 K in an isolated cell (~50 μm), the temperature changes can reach 1-2 K at tissue length-scales of

~10 mm. Overall, the detection limit required for the measurement of endogenous temperature changes at tissue length-scales are in the order of ~0.1 K, which is realizable in common macroscopic measurement techniques.

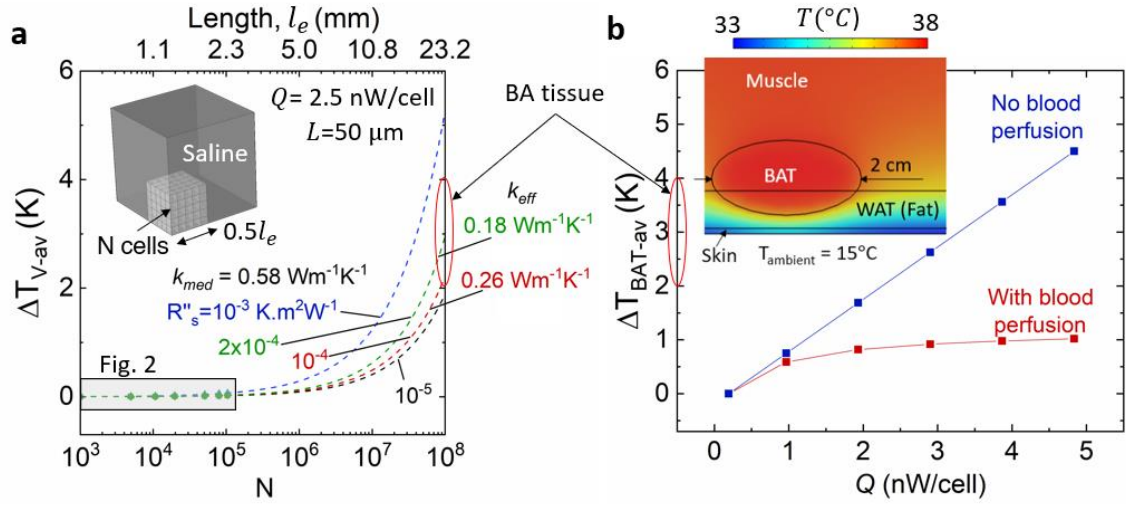

Figure 6. a) Average temperature of the stack of cells increases with the number of cells, N, and reaches ~2-4 K at a length-scale of ~20 mm. We extrapolated these curves from Figure 2. b) Average temperature change in the BAT deposit is shown for 5, 10, 15, 20, 25-fold increase in BAT metabolism. The x-axis shows the heat released in the tissue in nW per cell (of dimension 50 µm x 50 µm x 50 µm). The "no blood perfusion" case assumed ω_b to be zero. More details on this bio-heat transport model can be found in the supplementary material.

Choosing an appropriate thermometry technique

In the previous section, we estimated the typical endogenous temperature changes at intracellular and tissue length-scales. Such temperature changes occur inherently in the biological medium, irrespective of the measurement technique. When a temperature probe is introduced into the biological milieu, it often measures a temperature that is spatially averaged across the dimensions of the probe [69]. Therefore, in this section, we consider the perspective of the measurement technique and examine the temperature changes measured by the probes employed. Specifically, we consider two commonly used techniques – intracellular and extracellular thermometry. We examine the expected measurement temperatures over a range of cellular to tissue length-scales for biochemical reactions of different timescales and heat rates. Such an analysis would help to identify the optimal thermometry technique that can provide physiological insight for a given type of biochemical reaction.

Figure 7 schematically depicts the two measurement techniques that we analyze in this section. We define ΔT_{int} as the maximum intracellular temperature that can be measured through infinitesimal intracellular probes (say nanoparticles or molecular probes) dispersed inside the cells at the surface of a tissue of N cells. We define ΔT_{ext}, as the temperature measured by an extracellular probe (say RTD or thermocouple) of 50×50×50 µm^3 size, which is also assumed to

be at the surface of a tissue of N cells. In the following sections, we first analyze the time-scale effects of the measurement temperatures (ΔT_{int} vs. ΔT_{ext}) across a range of length-scales. We then highlight how the temperature changes compare with the typical detectable limits of the measurement techniques.

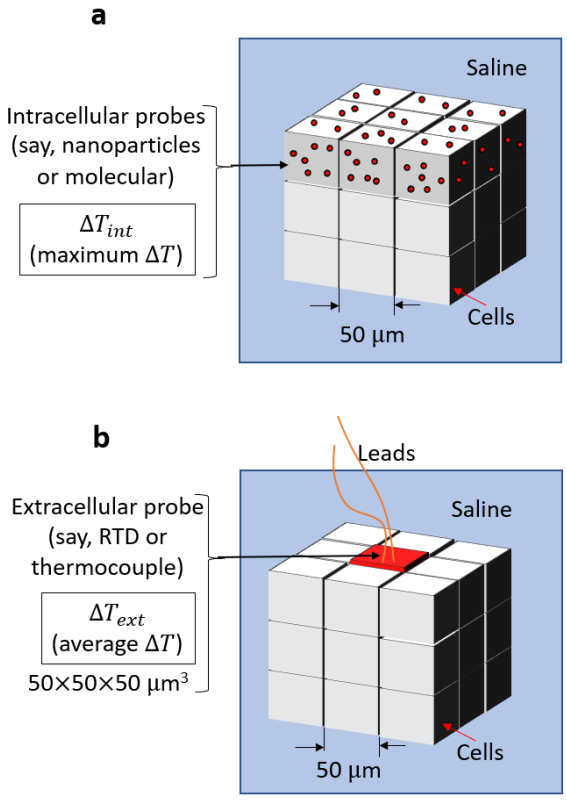

Figure 7 a) Schematic of intracellular temperature measurement is shown, defining ΔT_{int} as the maximum intracellular temperature from cells at the surface of N number of cells. b) Schematic of a typical extracellular temperature measurement is shown, defining ΔT_{ext} as the extracellular temperature measured at a location of size (50×50×50 μm^3). The probe is assumed to have the same thermal properties as that of water. We assume a nominal resistance, R_S'' = 10^{-4} K.m^{2}W^{-1} corresponding to a k_{eff}~0.26 Wm^{-1}K^{-1}.

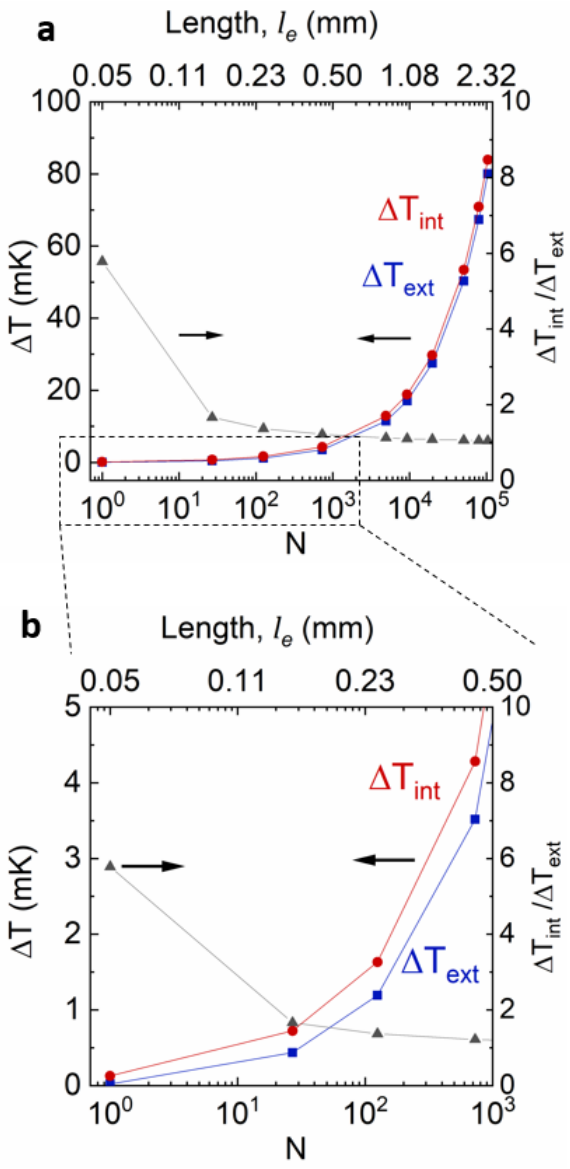

Figure 8 a) The extracellular (ΔT_{ext}, blue points) and intracellular (ΔT_{int}, red points) temperature changes during endogenous thermogenesis (10 nW, steady state per cell) are plotted on the left y-axis. The ratio $\Delta T_{int}/\Delta T_{ext}$ (black points) is plotted on the right y-axis. b) The temperature changes over N=1 to 1000 is plotted separately to clearly show the magnitude of temperature changes at small length-scales. We assumed the cell to have edge length L=50 μm. The ratio $\Delta T_{int}/\Delta T_{ext}$ is independent of the magnitude of heat.

Time-scale effects

We first compare the steady-state temperature changes expected to be measured by extracellular (ΔT_{ext}) and intracellular (ΔT_{int}) probes, as shown in Figure 8. We assume a steady heat release of 10 nW per cell of size 50 μm, typical of brown adipose tissue cells under cold-induced thermogenesis. From Figure 8, we find that the ΔT_{ext} and ΔT_{int} closely follow each other on the

scale of 0 to 100 mK over a range of length-scales. For N<1000, the absolute magnitude of the temperature changes is < 10 mK, which is lower than the typical detection limits of the measurement techniques. We later discuss (in the following section) the influence of the heat magnitude on the absolute value of the temperatures and how they compare against the detection limit. In Figure 8, we also plot the ratio of the temperature changes, $\Delta T_{int}/\Delta T_{ext}$, which is independent of the absolute magnitude of heat release. The ratio $\Delta T_{int}/\Delta T_{ext}$ reaches a maximum of about 5.8 at N=1, which corresponds to an isolated cell. Further, $\Delta T_{int}/\Delta T_{ext}$ remains under 2 for N>25 cells. This shows that using an intracellular probe to measure temperature changes is beneficial, especially if the number of cells in the study is less than 10. In other words, intracellular probes can be useful for *in vitro* studies in a petri dish setting, where the temperature changes inside a cell can be up to 5.8 times higher than that outside of a cell, under steady-state conditions.

Under transient heating conditions, intracellular temperature changes (ΔT_{int}) can be 5-20 times higher than that measured at extracellular regions (ΔT_{ext}) in an *in vitro* setting for isolated cells. We depict this in Figure 9, where we show the simulated measurement temperatures for transient heating of $Q = 10\ e^{-t/\tau}$nW in a single isolated cell in an infinite medium, releasing heat Q at different timescales (τ). We find the ratio $\Delta T_{int}/\Delta T_{ext}$ to increase from 5.8 (~for steady-state conditions) to up to 18 at a timescale of τ=1 ms for the heat release. The ratio $\Delta T_{int}/\Delta T_{ext}$ is high at lower timescales (τ) primarily because the time taken for the heat to diffuse (given by L^2/α, where L is the length-scale and α is the thermal diffusivity) and reach the extracellular probes is higher than the heat release duration (τ). Thus, the heat is spatially confined to intracellular regions. Intracellular thermometry is, therefore, better suited in isolated cells *in vitro*, especially if the heat release is expected to be transient with a timescale ≪ 1 s.

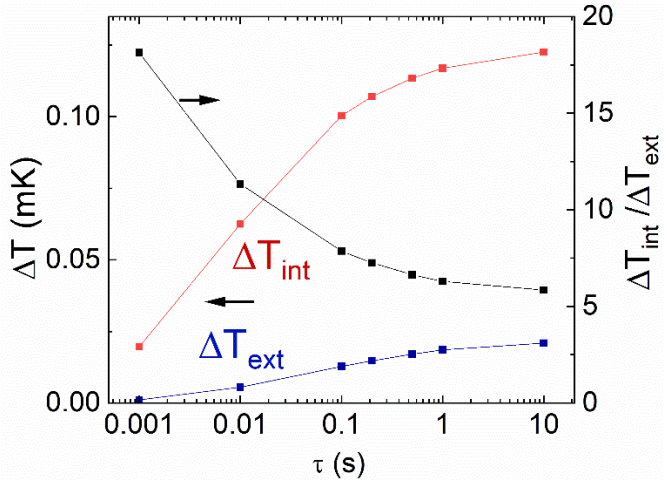

Figure 9: The intracellular (ΔT_{int}, red) and extracellular (ΔT_{ext}, blue) temperature changes are plotted along the left y-axis for a transient heat release (10 $e^{-t/\tau}$ nW) in an isolated cell in an infinite saline medium. The ratio $\Delta T_{int}/\Delta T_{ext}$ (black points) is plotted on the right y-axis. The ratio $\Delta T_{int}/\Delta T_{ext}$ is independent of the magnitude of heat.

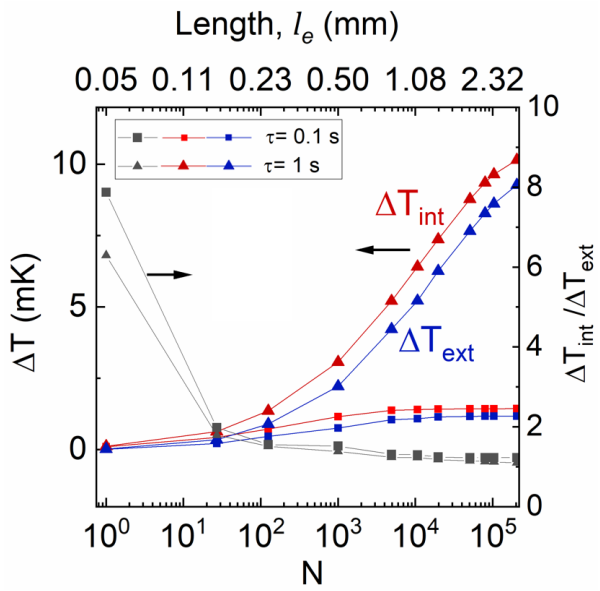

Figure 10. The extracellular (ΔT_{ext}, blue points) and intracellular (ΔT_{int}, red points) temperature changes during transient thermogenesis (10 $e^{-t/\tau}$nW per cell) are plotted on the left y-axis. The ratio $\Delta T_{int}/\Delta T_{ext}$ (black points) is plotted on the right y-axis. We assumed the cell to have edge length L=50 μm and R_S''~10^{-4} K.m^{2}W^{-1}. The ratio $\Delta T_{int}/\Delta T_{ext}$ is independent of the magnitude of heat.

Since the transient heating is localized within a cell, the transient temperature changes do not increase at larger length-scales. In Figure 6 and Figure 8, the steady-state heating resulted in the corresponding temperature change (ΔT) to increase with the number of cells (N) as $\Delta T \sim N^{\gamma}$. However, if the heat release is transient in nature, as shown in Figure 10, the corresponding temperature changes do not increase with the number of cells (N) beyond a certain N. Moreover, from Figure 10, we find that a smaller timescale of heat release (τ~0.1 s) results in temperature changes that saturate at smaller length-scales (l_e~1 mm) than that for τ~1 s. This is expected since the heat diffusion length ($\sqrt{\alpha\tau}$) is smaller for shorter heat release duration (τ). Overall, we again find that intracellular thermometry is better suited for transiently thermogenic reactions with timescales $\ll$ 1 s in isolated cells under *in vitro* conditions; however, at larger length-scales, extracellular thermometry is also equally suited to measure the temperature changes since $\Delta T_{int}/\Delta T_{ext} \rightarrow 1$ for length-scales l_e>0.2 mm. Throughout this section, we analyzed the ratio $\Delta T_{int}/\Delta T_{ext}$ to conclude that intracellular thermometry is better suited for transients in isolated cells; however, the absolute magnitude of ΔT_{int} is < 1 mK (Figures 8-10) in isolated cells, which renders it not possible to measure using conventional techniques. We discuss the implications of the absolute temperature changes and the heat rate magnitudes in the following section.

Heat rate magnitude: endogenous vs stimulated

Under physiological conditions, intracellular temperature changes are usually limited to sub-mK values, which are not directly measurable *in vitro* by intracellular probes, unless the cells are thermally isolated by multiple vacuum chambers [41], [42]. However, if the intracellular heat release can be stimulated by external agents, the intracellular temperature changes can reach

measurable limits, as we show in Figure 11. We plot the steady-state temperature changes (ΔT_{int} and ΔT_{ext}) in an isolated cell in a petri dish setting, for a range of uniform volumetric heat release Q inside the cell. Typically, any physiological heat release rate is < 100 nW [28], [41], [42], [62] as marked in Figure 11. To increase the expected temperatures to measurable limits (conservatively, 0.1 K), the intracellular heat release needs to be stimulated exogenously to > 10 μW. Stimulated mitochondrial proton uncoupling [9] is one such example, where the heat release is stimulated by an external proton uncoupler. Other examples of exogenous heating include laser [65], resonating magnetic nanoparticles [36], norepinephrine [64], etc. Only when the intracellular heat release is stimulated, intracellular thermometry techniques can provide useful and measurable physiological information on the stimulated biochemical reaction. Therefore, intracellular temperature probes can be useful for steady-state and transient measurements *in vitro*, especially if the intracellular heat release is stimulated exogenously.

On the other hand, extracellular thermometry can be useful for probing endogenously thermogenic reactions at tissue length-scales. The steady-state temperature changes increase with the length-scale and reach up to a few K at l_e~10 mm, as evident from Figure 6. At such length-scales (l_e> 10 mm), the extracellular probe can directly measure thermogenesis-induced temperature changes. Further, there is little benefit to using intracellular probes at larger length-scales (> 1 mm) as evident from Figure 8a. Therefore, extracellular temperature probes can provide useful physiological information on endogenous thermogenesis-related activities at larger length-scales such as tissues/organs that are $>$ 1 mm. This is also evident from previous studies that utilized mm-scale thermometers to study thermoregulatory neuronal circuits [4], [5], and cancer metabolism [6], [29], [70], [71].

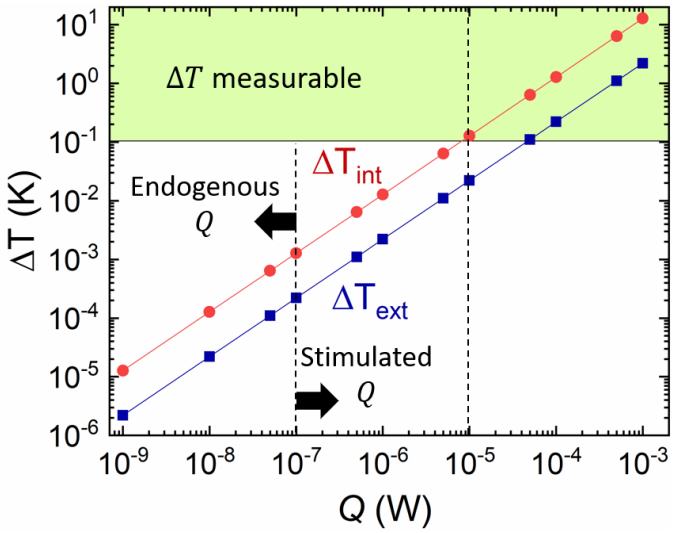

Figure 11. For a single isolated cell in a typical petri dish setting, the intracellular (ΔT_{int}, red) and extracellular (ΔT_{ext}, blue) temperature changes are plotted for various steady-state volumetric heat release rates, Q. Physiologically expected heat release rates are $\ll$ 100 nW. The typical intracellular temperature measurement limit is > 0.1 K, in an *in vitro* petri dish setting.

SUMMARY OF DISCUSSION

In the discussions above, we explained how our heat diffusion model can be used to design cellular thermometry experiments. Here, we first summarize our key recommendations, provide relevant examples, and then address some limitations. We explored different thermometry options and thermogenic reactions of different heat rates and times-scales to identify which technique is optimal for a given reaction. By investigating a range of parameters such as length-scales, timescales, and expected heat release rates, we find the following:

1. Intracellular thermometry is useful in a petri dish setting for *in vitro* studies, especially if the intracellular heat release is stimulated exogenously and is transient in nature occurring over < 1 s. For instance, a previous study utilized a nanodiamond-based intracellular thermometer and laser-induced heating to find that the early embryonic development in *C. elegans* is determined independently by individual cells rather than cell-to-cell communications [72]. Another study utilized a microfabricated intracellular thermometer in *Aplysia* neurons and observed transient heating during sudden mitochondrial depolarization by proton uncoupler BAM15 [9]. Such intracellular thermometry studies utilizing exogenous stimulants can result in temperature changes above detection limits and provide unprecedented insights into the subcellular metabolic pathways.
2. Extracellular thermometry is useful to observe physiologically relevant and endogenous thermogenesis, especially in tissues (> 1 mm length-scale). For instance, a previous study utilized an extracellular thermistor probe to observe that the brown adipose tissue (BAT) thermogenesis is controlled by a synergy between Leptin and thyrotropin-releasing hormone in the rat's hindbrain [5]. Another study observed that the hypothalamic orexin-synthesizing neurons contribute to the intensity with which rats respond to external conditions, by measuring BAT temperatures through a thermistor [73]. Since the endogenous temperature changes in tissues [1], [2], [6] can be above the detection limits, they can provide direct insights into the metabolic pathways being probed.

Other non-conventional thermometry techniques such as isolating a cell in a microfluidic channel or micropipettes with multiple isothermal vacuum chambers have been previously attempted [41], [42]. Such techniques increase the resistance to heat flow, which can increase the temperature changes above detection limits even for a nominal endogenous heat release ~1-10 nW from one or few cells. However, under such isolated conditions, transient temperature measurements in the order of sub-seconds are yet to be developed. Overall, future bioenergetics studies can choose an appropriate thermometry technique using our guidelines discussed here, if the underlying biochemical reaction's timescale and stimulation mechanisms are known.

Throughout this work, we utilized a cellular heat diffusion model with a cuboidal network of resistance R_s'' to capture the influence of interfacial resistances in the cellular milieu. We assumed a constant k_{med} of 0.58 $Wm^{-1}K^{-1}$ corresponding to water (k_{water}) and concentrated all the resistances from the proteins or organelles to be at R_s''. However, cellular heat diffusion could be from a combination of k_{med} ($< k_{water}$, due to a homogeneous distribution of proteins and ions or low packing density) and R_s'', where the magnitude of $R_s''(=\sum_i R_{TIR_i})$ could be less than that

used throughout this work. Similarly, the increase in thermal conductivity at large length-scales could be due to a low packing density of cells in tissues. Further, lipid bilayers and other proteins undergo phase change near room temperatures [74], [75], which may influence the local thermal resistances. Thus, the effective thermal conductivity (k_{eff}) may likely depend not only on the length-scale but also on the temperature at which they are measured. Future intracellular thermometry studies can provide insights on the length-scale and temperature dependence of thermal properties (k_{eff} and R_S'') by measuring the local temperature changes across a range of length-scales 50 nm – 100 μm using a certain heat input. Spatial distribution of the local thermal interfacial resistances can be known if spatial temperature distributions can also be measured across the cellular medium. Recent studies [59], [76] have measured the thermal properties of the lipid bilayers in cell membranes; however, measurements on cytoskeleton components such as actin, microtubules, intermediate filaments, etc. are necessary to understand the significance of their thermal interfacial resistance. Additional topographical information on the biomolecular interfaces and their interface resistance values may help to improve the heat diffusion model. Nonetheless, the cuboidal resistance network used in this work served as a generalized example to understand the influence of the interface resistances.

CONCLUSION

In conclusion, our work provides recommendations on choosing a thermometry technique by quantifying whether/when temperature changes are measurable under different biological conditions. A cellular heat diffusion model that incorporates the effects of dissimilar interfaces, provides the temperatures estimated in this work. We show that the commonly used effective thermal conductivity parameter may fail to capture true temperature distributions in the cellular milieu. This is particularly true at sub-cellular length scales where local interfacial resistances can be in the order of 10^{-7}-10^{-6} $K.m^2W^{-1}$, which can result in an effective thermal conductivity (k_{eff}) substantially lower than those of the medium (k_{med}) and proteins (k_p). We captured the reduction in thermal conductivity at lower length-scales, as a test case, using a cuboidal topology for the interfacial resistance network. Our results underscore the need for future studies to measure and map the thermal interfacial resistances in the cellular medium. Further, we find that in subcellular organelles, temperature changes are expected to be less than 100 mK under physiological conditions. In contrast, at tissue scales, we find that even endogenous heat of few nanowatts per cell can produce 1-2 K overall temperature change, which is typical in cold-induced thermogenesis. Thus, extracellular probes are better suited to probing endogenous thermogenic reactions, since the temperature changes exceed detection limits at tissue length-scales. On the other hand, intracellular thermometry is better suited to probing transient thermogenic reactions since transient temperature changes are typically localized within the cell. However, such intracellular temperature changes are measurable only if the biochemical reaction is stimulated exogenously. Overall, this work provides insight into cellular heat diffusion modeling, using which we show how to choose the right thermometry technique to probe a biochemical pathway.

Supplementary material:

A supplementary material document accompanies this paper.

Acknowledgments:

We thank Dr. Jeffrey Brown, Prof. Daniel Llano, and Prof. Rhanor Gillette for their useful inputs throughout this work. Figure 1 was made in part using biorender.com. This work was supported in part by funding from the National Science Foundation through Grant No. NSF-CBET-17-06854.

Ethics declaration

The authors declare that they do not have any conflict of interest.

References:

[1] U. R. Acharya, E. Y. K. Ng, J.-H. Tan, and S. V. Sree, "Thermography based breast cancer detection using texture features and Support Vector Machine," *J Med Syst*, vol. 36, no. 3, Art. no. 3, Jun. 2012, doi: 10.1007/s10916-010-9611-z.

[2] A. Helmy, M. Holdmann, and M. Rizkalla, "Application of thermography for non-invasive diagnosis of thyroid gland disease," *IEEE Trans Biomed Eng*, vol. 55, no. 3, Art. no. 3, Mar. 2008, doi: 10.1109/TBME.2008.915731.

[3] C. Guy, F. Kaplan, J. Kopka, J. Selbig, and D. K. Hincha, "Metabolomics of temperature stress," *Physiol Plant*, vol. 132, no. 2, Art. no. 2, Feb. 2008, doi: 10.1111/j.1399-3054.2007.00999.x.

[4] S. F. Morrison, C. J. Madden, and D. Tupone, "Central Neural Regulation of Brown Adipose Tissue Thermogenesis and Energy Expenditure," *Cell Metabolism*, vol. 19, no. 5, pp. 741–756, May 2014, doi: 10.1016/j.cmet.2014.02.007.

[5] R. C. Rogers, M. J. Barnes, and G. E. Hermann, "Leptin 'gates' thermogenic action of thyrotropin-releasing hormone in the hindbrain," *Brain Research*, vol. 1295, pp. 135–141, Oct. 2009, doi: 10.1016/j.brainres.2009.07.063.

[6] P. M. Gullino, R. K. Jain, and F. H. Grantham, "Temperature Gradients and Local Perfusion in a Mammary Carcinoma," *J Natl Cancer Inst*, vol. 68, no. 3, pp. 519–533, Mar. 1982, doi: 10.1093/jnci/68.3.519.

[7] K. Okabe, N. Inada, C. Gota, Y. Harada, T. Funatsu, and S. Uchiyama, "Intracellular temperature mapping with a fluorescent polymeric thermometer and fluorescence lifetime imaging microscopy," *Nat Commun*, vol. 3, p. 705, Feb. 2012, doi: 10.1038/ncomms1714.

[8] S. Kiyonaka *et al.*, "Genetically encoded fluorescent thermosensors visualize subcellular thermoregulation in living cells," *Nat. Methods*, vol. 10, no. 12, Art. no. 12, Dec. 2013, doi: 10.1038/nmeth.2690.

[9] M. C. Rajagopal *et al.*, “Transient heat release during induced mitochondrial proton uncoupling,” *Communications Biology*, vol. 2, no. 1, Art. no. 1, Jul. 2019, doi: 10.1038/s42003-019-0535-y.
[10] J. Zhou, B. del Rosal, D. Jaque, S. Uchiyama, and D. Jin, “Advances and challenges for fluorescence nanothermometry,” *Nature Methods*, vol. 17, no. 10, Art. no. 10, Oct. 2020, doi: 10.1038/s41592-020-0957-y.
[11] R. Tanimoto *et al.*, “Detection of Temperature Difference in Neuronal Cells,” *Scientific reports*, vol. 6, p. 22071, Mar. 2016, doi: 10.1038/srep22071.
[12] T. Tsuji, K. Ikado, H. Koizumi, S. Uchiyama, and K. Kajimoto, “Difference in intracellular temperature rise between matured and precursor brown adipocytes in response to uncoupler and β-adrenergic agonist stimuli,” *Scientific Reports*, vol. 7, no. 1, Art. no. 1, Oct. 2017, doi: 10.1038/s41598-017-12634-7.
[13] W. Tian *et al.*, “A high precision apparatus for intracellular thermal response at single-cell level,” *Nanotechnology*, vol. 26, no. 35, Art. no. 35, Aug. 2015, doi: 10.1088/0957-4484/26/35/355501.
[14] C. Wang *et al.*, “Determining intracellular temperature at single-cell level by a novel thermocouple method,” *Cell Res.*, vol. 21, no. 10, Art. no. 10, Oct. 2011, doi: 10.1038/cr.2011.117.
[15] S. Arai, S.-C. Lee, D. Zhai, M. Suzuki, and Y. T. Chang, “A Molecular Fluorescent Probe for Targeted Visualization of Temperature at the Endoplasmic Reticulum,” *Scientific Reports*, vol. 4, no. 1, Art. no. 1, Oct. 2014, doi: 10.1038/srep06701.
[16] Y. Takei *et al.*, “A Nanoparticle-Based Ratiometric and Self-Calibrated Fluorescent Thermometer for Single Living Cells,” *ACS Nano*, vol. 8, no. 1, pp. 198–206, Jan. 2014, doi: 10.1021/nn405456e.
[17] D. Chrétien *et al.*, “Mitochondria are physiologically maintained at close to 50 °C,” *PLOS Biology*, vol. 16, no. 1, p. e2003992, Jan. 2018, doi: 10.1371/journal.pbio.2003992.
[18] G. Baffou, H. Rigneault, D. Marguet, and L. Jullien, “A critique of methods for temperature imaging in single cells,” *Nat. Methods*, vol. 11, no. 9, Art. no. 9, Sep. 2014, doi: 10.1038/nmeth.3073.
[19] G. Baffou, H. Rigneault, D. Marguet, and L. Jullien, “Reply to: ‘Validating subcellular thermal changes revealed by fluorescent thermosensors’ and ‘The 10 5 gap issue between calculation and measurement in single-cell thermometry,’” *Nature Methods*, vol. 12, no. 9, Art. no. 9, Sep. 2015, doi: 10.1038/nmeth.3552.
[20] S. Kiyonaka, R. Sakaguchi, I. Hamachi, T. Morii, T. Yoshizaki, and Y. Mori, “Validating subcellular thermal changes revealed by fluorescent thermosensors,” *Nature Methods*, vol. 12, no. 9, Art. no. 9, Sep. 2015, doi: 10.1038/nmeth.3548.
[21] M. Suzuki, V. Zeeb, S. Arai, K. Oyama, and S. Ishiwata, “The 105 gap issue between calculation and measurement in single-cell thermometry,” *Nat Methods*, vol. 12, no. 9, Art. no. 9, Sep. 2015, doi: 10.1038/nmeth.3551.
[22] A. D. Pickel, A. Teitelboim, E. M. Chan, N. J. Borys, P. J. Schuck, and C. Dames, “Apparent self-heating of individual upconverting nanoparticle thermometers,” *Nature Communications*, vol. 9, no. 1, Art. no. 1, Nov. 2018, doi: 10.1038/s41467-018-07361-0.
[23] A. Vyšniauskas, M. Qurashi, N. Gallop, M. Balaz, H. L. Anderson, and M. K. Kuimova, “Unravelling the effect of temperature on viscosity-sensitive fluorescent molecular rotors,” *Chemical Science*, vol. 6, no. 10, pp. 5773–5778, 2015, doi: 10.1039/C5SC02248G.

[24] D. Chrétien *et al.*, “Pitfalls in Monitoring Mitochondrial Temperature Using Charged Thermosensitive Fluorophores,” *Chemosensors*, vol. 8, no. 4, Art. no. 4, Dec. 2020, doi: 10.3390/chemosensors8040124.
[25] G. Baffou, I. Bordacchini, A. Baldi, and R. Quidant, “Simple experimental procedures to distinguish photothermal from hot-carrier processes in plasmonics,” *Light: Science & Applications*, vol. 9, no. 1, Art. no. 1, Jun. 2020, doi: 10.1038/s41377-020-00345-0.
[26] M. Suzuki and T. Plakhotnik, “The challenge of intracellular temperature,” *Biophys Rev*, vol. 12, no. 2, pp. 593–600, Apr. 2020, doi: 10.1007/s12551-020-00683-8.
[27] J. Crezee and J. J. W. Lagendijk, “Experimental verification of bioheat transfer theories: measurement of temperature profiles around large artificial vessels in perfused tissue,” *Phys. Med. Biol.*, vol. 35, no. 7, pp. 905–923, Jul. 1990, doi: 10.1088/0031-9155/35/7/007.
[28] D. B. Rodrigues *et al.*, “Numerical 3D modeling of heat transfer in human tissues for microwave radiometry monitoring of brown fat metabolism,” *Proc SPIE*, vol. 8584, Feb. 2013, doi: 10.1117/12.2004931.
[29] R. K. Jain, F. H. Grantham, and P. M. Gullino, “Blood Flow and Heat Transfer in Walker 256 Mammary Carcinoma,” *J Natl Cancer Inst*, vol. 62, no. 4, pp. 927–933, Apr. 1979, doi: 10.1093/jnci/62.4.927.
[30] P. Kapitza, “The study of heat transfer in helium II,” *J. Phys.(Moscow)*, vol. 4, p. 181, 1941.
[31] Z. Ge, D. G. Cahill, and P. V. Braun, “AuPd Metal Nanoparticles as Probes of Nanoscale Thermal Transport in Aqueous Solution,” *J. Phys. Chem. B*, vol. 108, no. 49, pp. 18870–18875, Dec. 2004, doi: 10.1021/jp048375k.
[32] O. M. Wilson, X. Hu, D. G. Cahill, and P. V. Braun, “Colloidal metal particles as probes of nanoscale thermal transport in fluids,” *Phys. Rev. B*, vol. 66, no. 22, p. 224301, Dec. 2002, doi: 10.1103/PhysRevB.66.224301.
[33] Z. Ge, D. G. Cahill, and P. V. Braun, “Thermal Conductance of Hydrophilic and Hydrophobic Interfaces,” *Phys. Rev. Lett.*, vol. 96, no. 18, p. 186101, May 2006, doi: 10.1103/PhysRevLett.96.186101.
[34] H. M. Duong, D. V. Papavassiliou, K. J. Mullen, B. L. Wardle, and S. Maruyama, “A numerical study on the effective thermal conductivity of biological fluids containing single-walled carbon nanotubes,” *International Journal of Heat and Mass Transfer*, vol. 52, no. 23, pp. 5591–5597, Nov. 2009, doi: 10.1016/j.ijheatmasstransfer.2009.06.016.
[35] K. Khosla, L. Zhan, A. Bhati, A. Carley-Clopton, M. Hagedorn, and J. Bischof, “Characterization of Laser Gold Nanowarming: A Platform for Millimeter-Scale Cryopreservation,” *Langmuir*, vol. 35, no. 23, pp. 7364–7375, Jun. 2019, doi: 10.1021/acs.langmuir.8b03011.
[36] N. Manuchehrabadi *et al.*, “Improved tissue cryopreservation using inductive heating of magnetic nanoparticles,” *Science Translational Medicine*, vol. 9, no. 379, Mar. 2017, doi: 10.1126/scitranslmed.aah4586.
[37] E. M. Knavel and C. L. Brace, “Tumor Ablation: Common Modalities and General Practices,” *Tech Vasc Interv Radiol*, vol. 16, no. 4, pp. 192–200, Dec. 2013, doi: 10.1053/j.tvir.2013.08.002.
[38] G. Poggi, N. Tosoratti, B. Montagna, and C. Picchi, “Microwave ablation of hepatocellular carcinoma,” *World J Hepatol*, vol. 7, no. 25, pp. 2578–2589, Nov. 2015, doi: 10.4254/wjh.v7.i25.2578.

[39] D. Li, J. Kang, B. J. Golas, V. W. Yeung, and D. C. Madoff, "Minimally invasive local therapies for liver cancer," *Cancer Biol Med*, vol. 11, no. 4, pp. 217–236, Dec. 2014, doi: 10.7497/j.issn.2095-3941.2014.04.001.
[40] M. C. Rajagopal, K. V. Valavala, D. Gelda, J. Ma, and S. Sinha, "Fabrication and characterization of thermocouple probe for use in intracellular thermometry," *Sensors and Actuators A: Physical*, vol. 272, pp. 253–258, Apr. 2018, doi: 10.1016/j.sna.2018.02.004.
[41] S. Hong *et al.*, "Sub-nanowatt microfluidic single-cell calorimetry," *Nature Communications*, vol. 11, no. 1, Art. no. 1, Jun. 2020, doi: 10.1038/s41467-020-16697-5.
[42] S. Hur, R. Mittapally, S. Yadlapalli, P. Reddy, and E. Meyhofer, "Sub-nanowatt resolution direct calorimetry for probing real-time metabolic activity of individual C. elegans worms," *Nature Communications*, vol. 11, no. 1, Art. no. 1, Jun. 2020, doi: 10.1038/s41467-020-16690-y.
[43] A. S. Verkman, "Solute and macromolecule diffusion in cellular aqueous compartments," *Trends in Biochemical Sciences*, vol. 27, no. 1, pp. 27–33, Jan. 2002, doi: 10.1016/S0968-0004(01)02003-5.
[44] G. Chen, "Ballistic-Diffusive Heat-Conduction Equations," *Phys. Rev. Lett.*, vol. 86, no. 11, pp. 2297–2300, Mar. 2001, doi: 10.1103/PhysRevLett.86.2297.
[45] C. Chen, Z. Du, and L. Pan, "Extending the diffusion approximation to the boundary using an integrated diffusion model," *AIP Advances*, vol. 5, no. 6, p. 067115, Jun. 2015, doi: 10.1063/1.4922269.
[46] G. Balasubramanian and I. K. Puri, "Heat conduction across a solid-solid interface: Understanding nanoscale interfacial effects on thermal resistance," *Appl. Phys. Lett.*, vol. 99, no. 1, p. 013116, Jul. 2011, doi: 10.1063/1.3607477.
[47] B. H. Kim, A. Beskok, and T. Cagin, "Molecular dynamics simulations of thermal resistance at the liquid-solid interface," *J. Chem. Phys.*, vol. 129, no. 17, p. 174701, Nov. 2008, doi: 10.1063/1.3001926.
[48] A. Rajabpour, R. Seif, S. Arabha, M. M. Heyhat, S. Merabia, and A. Hassanali, "Thermal transport at a nanoparticle-water interface: A molecular dynamics and continuum modeling study," *J. Chem. Phys.*, vol. 150, no. 11, p. 114701, Mar. 2019, doi: 10.1063/1.5084234.
[49] Y. Wang and P. Keblinski, "Role of wetting and nanoscale roughness on thermal conductance at liquid-solid interface," *Appl. Phys. Lett.*, vol. 99, no. 7, p. 073112, Aug. 2011, doi: 10.1063/1.3626850.
[50] L. Xue, P. Keblinski, S. R. Phillpot, S. U.-S. Choi, and J. A. Eastman, "Effect of liquid layering at the liquid–solid interface on thermal transport," *International Journal of Heat and Mass Transfer*, vol. 47, no. 19, pp. 4277–4284, Sep. 2004, doi: 10.1016/j.ijheatmasstransfer.2004.05.016.
[51] J.-L. BARRAT and F. CHIARUTTINI, "Kapitza resistance at the liquid—solid interface," *Molecular Physics*, vol. 101, no. 11, pp. 1605–1610, Jun. 2003, doi: 10.1080/0026897031000068578.
[52] A. Lervik, F. Bresme, and S. Kjelstrup, "Heat transfer in soft nanoscale interfaces: the influence of interface curvature," *Soft Matter*, vol. 5, no. 12, pp. 2407–2414, 2009, doi: 10.1039/B817666C.
[53] A. Lervik, F. Bresme, S. Kjelstrup, D. Bedeaux, and J. M. Rubi, "Heat transfer in protein – water interfaces," *Physical Chemistry Chemical Physics*, vol. 12, no. 7, pp. 1610–1617, 2010, doi: 10.1039/B918607G.

[54] M. C. Rajagopal, T. Man, A. Agrawal, G. Kuntumalla, and S. Sinha, “Intrinsic thermal interfacial resistance measurement in bonded metal–polymer foils,” *Review of Scientific Instruments*, vol. 91, no. 10, p. 104901, Oct. 2020, doi: 10.1063/5.0012404.
[55] S. Sotoma *et al.*, “In situ measurement of intracellular thermal conductivity using heater-thermometer hybrid diamond nanosensor,” *bioRxiv*, p. 2020.06.03.126789, Jun. 2020, doi: 10.1101/2020.06.03.126789.
[56] M. P. Clausen, H. Colin-York, F. Schneider, C. Eggeling, and M. Fritzsche, “Dissecting the actin cortex density and membrane-cortex distance in living cells by super-resolution microscopy,” *J. Phys. D: Appl. Phys.*, vol. 50, no. 6, p. 064002, Jan. 2017, doi: 10.1088/1361-6463/aa52a1.
[57] C. M. O’Connor, J. U. Adams, and J. Fairman, “Essentials of cell biology,” *Cambridge, MA: NPG Education*, vol. 1, p. 54, 2010.
[58] H. C. Chang *et al.*, “Composite Structured Surfaces for Durable Dropwise Condensation,” *International Journal of Heat and Mass Transfer*, vol. 156, p. 119890, Aug. 2020, doi: 10.1016/j.ijheatmasstransfer.2020.119890.
[59] A. R. N. Bastos *et al.*, “Thermal Properties of Lipid Bilayers Determined Using Upconversion Nanothermometry,” *Advanced Functional Materials*, vol. 29, no. 48, p. 1905474, 2019, doi: 10.1002/adfm.201905474.
[60] C. E. Hagberg *et al.*, “Flow Cytometry of Mouse and Human Adipocytes for the Analysis of Browning and Cellular Heterogeneity,” *Cell Reports*, vol. 24, no. 10, pp. 2746-2756.e5, Sep. 2018, doi: 10.1016/j.celrep.2018.08.006.
[61] M. C. Rajagopal *et al.*, “Materials-to-device design of hybrid metal-polymer heat exchanger tubes for low temperature waste heat recovery,” *International Journal of Heat and Mass Transfer*, vol. 143, p. 118497, Nov. 2019, doi: 10.1016/j.ijheatmasstransfer.2019.118497.
[62] M. D. Johnson, J. Völker, H. V. Moeller, E. Laws, K. J. Breslauer, and P. G. Falkowski, “Universal constant for heat production in protists,” *PNAS*, vol. 106, no. 16, pp. 6696–6699, Apr. 2009, doi: 10.1073/pnas.0902005106.
[63] R. P. Chhabra, *CRC Handbook of Thermal Engineering*. CRC Press, 2017.
[64] M. K. Sato *et al.*, “Temperature Changes in Brown Adipocytes Detected with a Bimaterial Microcantilever,” *Biophysical Journal*, vol. 106, no. 11, pp. 2458–2464, Jun. 2014, doi: 10.1016/j.bpj.2014.04.044.
[65] G. Kucsko *et al.*, “Nanometre-scale thermometry in a living cell,” *Nature*, vol. 500, no. 7460, Art. no. 7460, Aug. 2013, doi: 10.1038/nature12373.
[66] G. Baffou *et al.*, “Photoinduced Heating of Nanoparticle Arrays,” *ACS Nano*, vol. 7, no. 8, pp. 6478–6488, Aug. 2013, doi: 10.1021/nn401924n.
[67] P. Lee, K. K. Y. Ho, P. Lee, J. R. Greenfield, K. K. Y. Ho, and J. R. Greenfield, “Hot fat in a cool man: infrared thermography and brown adipose tissue,” *Diabetes, Obesity and Metabolism*, vol. 13, no. 1, pp. 92–93, Jan. 2011, doi: 10.1111/j.1463-1326.2010.01318.x.
[68] W. D. van Marken Lichtenbelt *et al.*, “Cold-Activated Brown Adipose Tissue in Healthy Men,” *New England Journal of Medicine*, vol. 360, no. 15, pp. 1500–1508, Apr. 2009, doi: 10.1056/NEJMoa0808718.
[69] A. D. Pickel and C. Dames, “Size and shape effects on the measured peak temperatures of nanoscale hotspots,” *Journal of Applied Physics*, vol. 128, no. 4, p. 045103, Jul. 2020, doi: 10.1063/5.0012167.

[70] R. K. Jain, S. A. Shah, and P. L. Finney, “Continuous Noninvasive Monitoring of pH and Temperature in Rat Walker 256 Carcinoma During Normoglycemia and Hyperglycemia,” *J Natl Cancer Inst*, vol. 73, no. 2, pp. 429–436, Aug. 1984, doi: 10.1093/jnci/73.2.429.
[71] P. M. Gullino, P.-N. Yi, and F. H. Grantham, “Relationship Between Temperature and Blood Supply or Consumption of Oxygen and Glucose by Rat Mammary Carcinomas,” *J Natl Cancer Inst*, vol. 60, no. 4, pp. 835–847, Apr. 1978, doi: 10.1093/jnci/60.4.835.
[72] J. Choi *et al.*, “Probing and manipulating embryogenesis via nanoscale thermometry and temperature control,” *PNAS*, vol. 117, no. 26, pp. 14636–14641, Jun. 2020, doi: 10.1073/pnas.1922730117.
[73] M. Mohammed, Y. Ootsuka, M. Yanagisawa, and W. Blessing, “Reduced brown adipose tissue thermogenesis during environmental interactions in transgenic rats with ataxin-3-mediated ablation of hypothalamic orexin neurons,” *American Journal of Physiology-Regulatory, Integrative and Comparative Physiology*, vol. 307, no. 8, pp. R978–R989, Aug. 2014, doi: 10.1152/ajpregu.00260.2014.
[74] S. Youssefian, N. Rahbar, C. R. Lambert, and S. Van Dessel, “Variation of thermal conductivity of DPPC lipid bilayer membranes around the phase transition temperature,” *Journal of The Royal Society Interface*, vol. 14, no. 130, p. 20170127, May 2017, doi: 10.1098/rsif.2017.0127.
[75] J. A. Kenar, “The use of lipids as phase change materials for thermal energy storage,” *Lipid Technology*, vol. 26, no. 7, pp. 154–156, 2014, doi: 10.1002/lite.201400037.
[76] A. R. N. Bastos *et al.*, “Thermal properties of lipid bilayers derived from the transient heating regime of upconverting nanoparticles,” *Nanoscale*, vol. 12, no. 47, pp. 24169–24176, 2020, doi: 10.1039/D0NR06989B.